JACS
JOURNAL OF THE AMERICAN CHEMICAL SOCIETY
pubs.acs.org/JACS
Article

Genetically Encoded Fluorogenic DNA Aptamers for Imaging Metabolite in Living Cells

Yuting Wu, Wentao Kong, Jacqueline Van Stappen, Linggen Kong, Zhimei Huang, Zhenglin Yang, Yu-An Kuo, Yuan-I Chen, Yujie He, Hsin-Chih Yeh, Ting Lu, and Yi Lu*

Cite This: J. Am. Chem. Soc. 2025, 147, 1529−1541
Read Online
ACCESS | Metrics & More | Article Recommendations | Supporting Information

ABSTRACT: Genetically encoded fluorescent protein and fluorogenic RNA sensors are indispensable tools for imaging biomolecules in cells. To expand the toolboxes and improve the generalizability and stability of this type of sensor, we report herein a genetically encoded fluorogenic DNA aptamer (GEFDA) sensor by linking a fluorogenic DNA aptamer for dimethylindole red with an ATP aptamer. The design enhances red fluorescence by 4-fold at 650 nm in the presence of ATP. Additionally, upon dimerization, it improves the signal-to-noise ratio by 2−3 folds. We further integrated the design into a plasmid to create a GEFDA sensor for sensing ATP in live bacterial and mammalian cells. This work expanded genetically encoded sensors by employing fluorogenic DNA aptamers, which offer enhanced stability over fluorogenic proteins and RNAs, providing a novel tool for real-time monitoring of an even broader range of small molecular metabolites in biological systems.

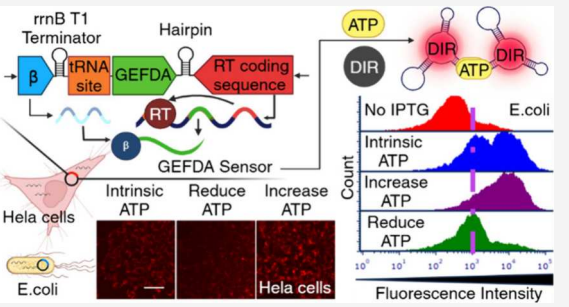

INTRODUCTION

Genetically encoded sensors employing fluorescent proteins have revolutionized biochemical and biomedical imaging. These protein-based sensors fuse fluorescent protein with a target molecule or a target-specific binding module via a short peptide linker.[1−3] The recognition of target molecules induces conformational changes in the protein construct[4−10] or regulates the synthesis of the fluorescent protein,[11−13] resulting in detectable fluorescence signal changes in living cells. Despite significant advancements in this field, developing protein-based sensors for diverse small-molecule analytes remains challenging due to the limited availability of proteins that bind a wide variety of small molecules and the time-consuming linker optimization.[14−16] Since numerous metabolites are present in cells, developing a method that can be generally applied to almost all metabolites is desirable. Toward this goal, fluorogenic RNAs combined with riboswitch added the toolbox of genetically encoded sensors for imaging small metabolites.[17−30] These fluorogenic RNAs undergo conformational changes upon binding to their targets, leading to an increase in fluorescence. Despite their adaptability to various analytes (e.g., SAM, TPP),[28,31] these fluorogenic RNA sensors have half-lives ranging from 0.25 to 1.25 h in cells.[32] While circularized RNA sensors extend their half-lives by 5- to 10-fold (7−10 h),[33] they still exhibit lower stability compared to protein sensors. Therefore, it is desirable to increase stability, while increasing the number of targets that genetically encoded sensors can detect in living cells.

Compared to riboswitches or RNA aptamers, DNA aptamers can be obtained more easily through the Systematic Evolution of Ligands by EXponential Enrichment (SELEX),[34,35] because the selection does not require reverse transcription. As a result, DNA aptamers that can bind a wide variety of targets, including small molecular metabolites, have been obtained and thus significantly expand the target molecules one can detect.[36−39] In addition, DNA aptamers also exhibit higher stability than proteins and RNAs,[40,41] positioning them as effective alternatives for metabolite sensing. Due to these advantages, DNA aptamers have been widely used to image and detect small molecules for over a decade.[42−57] Despite the above advantages and decades of research in this area, most DNA aptamer sensors for intracellular applications reported to date still require prelabeling with a fluorophore and then delivery into the cells. As a result, delivery efficiency and locations can vary widely. More importantly, since the cells are dividing and replicating, the delivered prelabeled DNA aptamers are constantly diluted, making them ineffective for long-term monitoring beyond the first generation of cells. To overcome these limitations and to maximize the full potential of DNA

Received: July 19, 2024
Revised: December 13, 2024
Accepted: December 16, 2024
Published: December 31, 2024

https://doi.org/10.1021/jacs.4c09855
J. Am. Chem. Soc. 2025, 147, 1529−1541

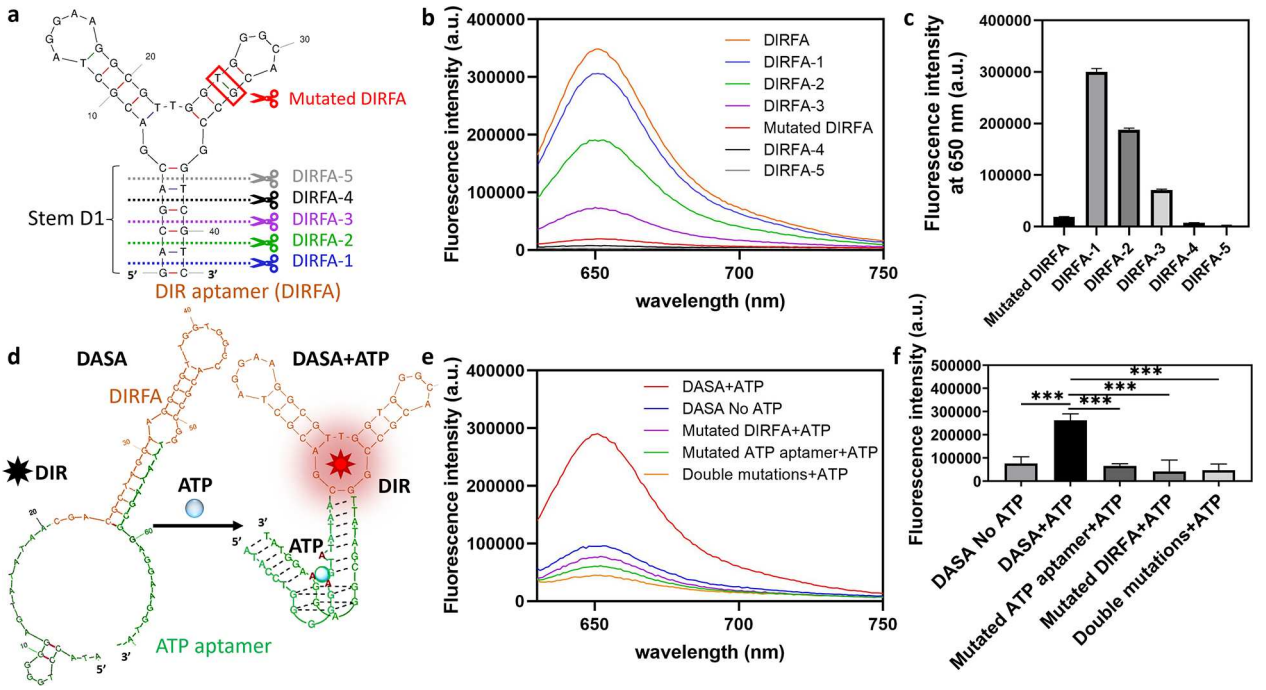

Figure 1. Design and Characterization of a DIRFA-based Split Aptamer (DASA) Sensor. **a)** A scheme that shows the designs of the truncational study for the dimethylindole red (DIR) specific Fluorogenic DNA Aptamer (DIRFA). DIRFA-1 to DIRFA-5 correspond to 1- to 5- base-pair truncation from the bottom of stem D1, respectively. Compared to the canonical DIRFA, the Mutated DIRFA lacks a T-G base pair (highlighted in the red box) but retains the stem D1. **b)** The spectrum of the truncated DIRFA showed a lower fluorescence intensity with a shorter stem length. **c)** The fluorescence intensity of truncated DIRFAs measured at 650 nm. **d)** The scheme of the DASA sensor. A split ATP aptamer (in green) was used to replace the stem D1. Without ATP (left), the stem structure is disrupted, and thus cannot interact with DIR. In the presence of ATP (right), the split ATP aptamer restores the stem structure with the structure switching upon binding to ATP. With the restored stem structure, DASA interacts with DIR and light up. **e)** The fluorometer recorded the spectrum of the DASA sensor with and without ATP incubations and its mutated controls with 5 mM ATP incubations. **f)** In the presence of 5 mM ATP, the DASA sensor showed a 244% increase in fluorescence intensity at 650 nm when compared to the group without ATP. However, point mutations in either split ATP aptamer, DIRFA, or both aptamers resulted in a constraint on the fluorescence increase. All the experiments were performed at room temperature upon excitation at 618 nm. ***, $p < 0.001$. Comparison was performed between DASA and groups carrying different mutations in DASA, or without ATP addition.

aptamers in imaging metabolites in cells, we are interested in developing a Genetically Encoded Fluorogenic DNA Aptamers (GEFDA) sensor that enables continuous expression of the aptamers even after cell division. However, to the best of our knowledge, GEFDA has never been demonstrated before.

The development of GEFDA sensors has two major challenges. First, although fluorogenic DNA aptamers such as those binding MG,[58,59] dapoxyl,[60] crystal violet,[61] Hoechst,[62] and Auramine O[63] have been developed for detecting small molecules in controlled environments,[60,63] most of their chromophores exhibit high autofluorescence, low specificity, high cytotoxicity, and poor signal-to-noise ratio (around or below 30% increase in fluorescence upon binding to their aptamers). The recent development of the Lettuce aptamer[64] employs chromophores with low cytotoxicity,[65−68] and was expressed in bacterial cells with a retron system.[69] However, this fluorogenic DNA aptamer has not been shown to work in mammalian cells, because of the differences in regulatory elements of gene expression between bacterial and mammalian cells, and thus limited its applications. More importantly, the fluorogenic aptamer needs to be coupled to a target recognition element to create GEFDA sensors for sensing metabolites.[70] It is challenging to express the coupled sensors that the binding of a target can transduce an increase of fluorescence signals inside the cells.

To meet these challenges, we report herein the first GEFDA sensor for imaging metabolites in live bacterial and mammalian cells. To achieve the goal, we first evaluated the fluorogenic Lettuce aptamer and dimethylindole red (DIR) specific Fluorogenic Aptamer (termed DIRFA hereafter),[71] and identified DIRFA as an excellent choice of fluorogenic aptamer in living cells, as it displays a > 10-fold increase in red fluorescence at 650 nm compared to its mutated control in a buffer mimicking the cellular environment. Encouraged by the result, we coupled DIRFA with an ATP aptamer[72] to develop a DIRFA-based Split Aptamer (DASA), which turns bright red upon forming a DASA/DIR/ATP complex. To improve the signal-to-noise ratio and stability in living cells, we constructed a dimeric DASA (dDASA) with dual chromophore and analyte bindings. This dimeric dDASA construct exhibited a 60% increase in brightness compared to the monomeric DASA sensor and displayed responsive detection of ATP levels in cells over 5 h. By integrating dDASA into plasmids that encode reverse transcriptase and a single-stranded DNA binding protein β, we created the GEFDA sensor to image ATP in live bacterial and mammalian cells. This platform has the potential to be adapted to express other DNA aptamers for imaging different metabolites in cells.

RESULTS AND DISCUSSION

Development and Characterization of DIRFA-Based Split Aptamer (DASA) Sensors. To develop a fluorogenic DNA sensor for intracellular sensing and imaging, we started with the Lettuce aptamer[64] and the dimethylindole red (DIR)

https://doi.org/10.1021/jacs.4c09855
J. Am. Chem. Soc. 2025, 147, 1529−1541

specific Fluorogenic DNA Aptamer DIRFA.[71] The Lettuce aptamer exhibited a 5-fold and 7-fold increase in fluorescence at 505 nm when bound to DFHBI in HEPES buffer (40 mM HEPES, pH 7.5, adjusted with NaOH; 100 mM KCl; and 1 mM $MgCl_2$) and Tris buffer (100 mM NaCl; 20 mM Tris-HCl pH 7.4; 2 mM $MgCl_2$; 5 mM KCl; 1 mM $CaCl_2$), respectively, compared to the mutated control in which two conserved bases were altered to prevent target binding.[64] However, in PBS buffer, which displays pH and salinity closer to intracellular conditions, the fluorescence enhancement was minimal (See Figure S1a in the Supporting Information). In contrast, DIRFA showed a 7- to 11-fold increase in fluorescence when compared to its mutated control in PBS buffer (Figure S1b). These findings signify the potential of the DIRFA/DIR complex for cellular sensor applications.

To compare the performance and stability of the DIRFA with well-established RNA aptamers, we included the broccoli fluorogenic RNA as a benchmark.[66] We tested the fluorescence intensity of DIRFA and broccoli in 50% cell lysates in PBS buffer. We observed a decrease in fluorescence intensity for the broccoli aptamer starting within 40 min, while the fluorescence intensity of the fluorogenic aptamer DIRFA remained stable over a 4 h tracking period (Figure S2a). The linear regression of the fluorescence signal revealed a significant decrease in slope for the RNA Broccoli aptamer compared to the DNA DIRFA aptamer, suggesting higher stability for the DIRFA aptamer under the tested conditions (Figure S2b). Consequently, the DIRFA was selected as the signal output throughout this article.

To understand the function of stem D1, a truncational analysis was carried out by removing one base pair at a time (Figure 1a). Notably, removing more than 3 base pairs led to an 80% reduced fluorescence intensity at 650 nm when compared to the canonical DIRFA (Figure 1b−c). Based on this observation, we hypothesized that the stem D1 is critical for the light-up effect and could function as a transducer region when linked with a target recognition aptamer to develop a small-molecule sensor.

To test the above hypothesis, we chose the ATP aptamer as a proof of concept since the ATP aptamer has been extensively researched and applied in sensing fields.[73−77] We replaced the stem D1 with a split ATP aptamer[78,79] (Figure 1d). In the absence of ATP, the structure of stem D1 was disrupted since the two strands of the split ATP aptamer were not perfectly base paired with each other. In contrast, the binding of ATP stabilized this region, and hence, restored the fluorogenic property of the DIRFA. This design was termed as DIRFA-based Split Aptamer (DASA) sensor and showed a 244% fluorescence increase at 650 nm upon the addition of 5 mM ATP when excited at 618 nm and tested with a fluorometer (Figure 1e−f, using the same parameters hereafter unless specified otherwise). Introducing point mutations in either the split ATP aptamer, DIRFA, or both led to reduced fluorescence signal changes (Figure 1e−f). These results demonstrated that the DASA sensor is capable of sensing ATP in solution.

To optimize the performance of the DASA sensors for cellular applications, we systematically varied the length of the stem D1 region from 7 base pairs (bp) to 5, 3, and 2 bp, named DASA-1, DASA-2, DASA-3, and DASA-4, respectively (Figure S3a−d) and compared the increase of fluorescence signals upon adding 5 mM ATP in PBS buffer (Figure S3e−h). When the length was reduced from 7 bp to 5 bp and then to 3 bp, the fluorescence upon ATP binding increased from 25% to 168% and 256%, respectively. Further shortening the stem from 3 bases to 2 bases reduced the fluorescence enhancement to 194%. Notably, as the stem D1 region is shortened, the fluorescence intensity of the sensor decreases, reaching its lowest point at 3 base pairs. Surprisingly, the fluorescence partially recovers when the stem is further reduced to only 2 base pairs (Figure S3). We used UNAfold to evaluate the potential conformations of the sensor under the conditions of 137 mM Na^+ and 0 mM Mg^{2+}, matching the salt condition of the PBS buffer used in the experiments. The results indicate that as the stem shortens, the ΔG of the DIRFA structure increases, and the melting temperature decreases (Table S1), which suggests that the formation of the DIRFA structure is more difficult with shorter stems, consistent with the observed decrease in fluorescence and sensor response. However, the 3-base pair variant (DASA-3) is an exception, as it did not favor the DIRFA structure. The DIRFA structure was absent from the top 13 predicted conformations returned by the software, which may explain its lower fluorescence intensity compared to the 2-base pair design. Given the software's limitations, particularly its inability to account for ATP binding and concentration, further investigation is needed to fully understand this behavior.

The linear ranges of fluorescence intensity showed a small difference between DASA-2 (0.05−5 mM ATP), DASA-3 (0.05−25 mM ATP), and DASA-4 (0.05−2.5 mM ATP) (Figure S4a−c). The LOD values for DASA-2, DASA-3, and DASA-4 were 0.7 mM, 1.0 mM, and 0.6 mM, respectively (see Supporting Information for further discussion).

To evaluate sensor specificity for ATP over other nucleotides, we incubated the DASA sensors with UTP, CTP, and GTP. Minimal fluorescence was observed for these nucleotides, while ATP incubation produced a 9-fold increase in fluorescence intensity at 650 nm, demonstrating strong selectivity for ATP over other nucleotide triphosphates (Figure S4d−f). This selectivity aligns with previous findings for ATP-specific aptamers.[75] However, it is important to note that the sensor may also interact with other adenosine-containing molecules, as the ATP aptamer primarily recognizes the adenosine moiety of ATP.[72] Given that this ATP aptamer is well-characterized, we used it as a proof of concept to demonstrate the potential of our sensing platform.

We further assessed the performance of DIRFA and DASA sensors at 37 °C for potential cellular applications. The DIRFA showed a 23-fold fluorescence increase when compared with the mutated DRIFA at 37 °C (Figure S5). This increase is higher than the 8-fold increase at room temperature, indicating a better signal-to-noise ratio at 37 °C. While the fluorescence intensity of the DIRFA/DIR complex at 650 nm is comparable between both temperatures, most of the DASA sensors exhibited a 3−8-fold decrease in fluorescence intensity at 37 °C than at room temperature. Moreover, the fluorescence enhancement of DASA-2, DASA-3, and DASA-4 with ATP incubation was 20%−90% lower at 37 °C relative to room temperature. This reduction may be attributed to the compromised stability of the ATP aptamer structure at a higher temperature due to thermostability.[80]

Dimerization of the DASA Sensors. To enhance the stability, binding affinity, and brightness of DASA sensors for cellular applications, we explored the potential improvements achieved by dimerizing the sensors, linking two monomer units together[81−85] (Figure 2a). As a proof of concept, we dimerized

https://doi.org/10.1021/jacs.4c09855
J. Am. Chem. Soc. 2025, 147, 1529−1541

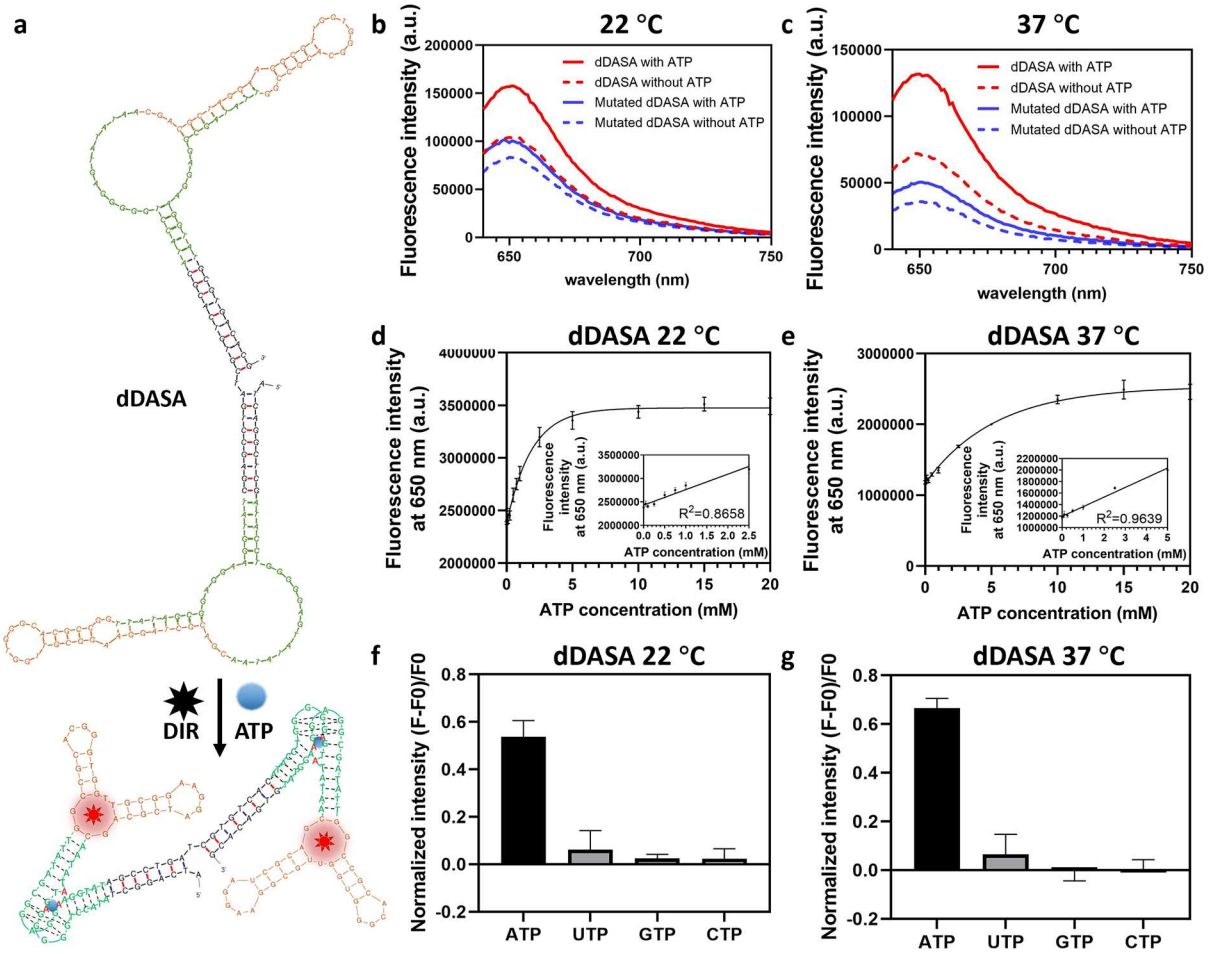

Figure 2. Design and Characterization of Dimeric DASA (dDASA) Sensors. **a)** A scheme that shows the design for the dimerization of the DASA sensor. **b)** The spectral analysis of dDASA 2-C and its mutant, which contains mutations in the binding site of the ATP aptamer, in the presence and absence of 5 mM ATP. The experiment was performed in the PBS buffer at room temperature (22 °C). **c)** The spectral analysis of dDASA 2-C and its mutant in PBS buffer at 37 °C in the presence and absence of 5 mM ATP. **d)** The detection range of dDASA 2-C under RT. **e)** The detection range of dDASA 2-C under 37 °C. **f)** The selectivity of dDASA 2-C over different rNTPs at RT. **g)** The selectivity of dDASA 2-C over different rNTPs under 37 °C. The fluorescence intensity was normalized to the group without the addition of rNTPs with the equation (F−F0)/F0, where F represents the fluorescence intensity at 650 nm in each group, and F0 represents the fluorescence intensity at 650 nm without the addition of any of these rNTPs.

DIRFA (Figure S6a) to evaluate the performance of the dimeric DIRFA (dDIRFA) relative to its monomeric form. In PBS buffer, dDIRFA demonstrated a 215% increase in fluorescence intensity at 650 nm compared to the mutated DIRFA. This increase mirrors the fluorescence difference observed between the monomeric DIRFA and its mutated form, suggesting that dimerization did not significantly affect fluorescence generation (Figure S6b).

To evaluate whether the dimerization has the potential to enhance the stability and performance of the fluorogenic aptamer under cellular environments, we compared the dimeric DIRFA (dDIRFA) and monomeric DIRFA in a 20% cell lysate environment. A 40% improvement in the signal-to-noise ratio, with a 35% increase in fluorescence intensity, was observed for dDIRFA compared to DIRFA (Figure S6c−d). To assess the stability of these sensors in cells, we delivered them into HEK293 cells. The signal-to-noise ratio, which measures the fluorescence difference between cells transfected with aptamers and those transfected with empty vehicles was compared. We observed a significantly higher signal-to-noise ratio for the fluorogenic DNA aptamers than that of the RNA aptamer. Specifically, the signal-to-noise ratios were 1.25 for broccoli RNA aptamer and 7.62 for DIRFA (Figure S7 0 h). Similar to the results observed in cell lysis, the dimerization of DIRFA resulted in an improved signal-to-noise ratio (9.59, Figure S7 0 h). To evaluate the stability of these fluorogenic aptamers in living cells, we monitored fluorescence over time. Seven hours post-transfection, the broccoli RNA no longer produced a signal above the noise level, while DIRFA and dDIRFA maintained signal-to-noise ratios of 6.08 and 10.09, respectively (Figure S7 7 h). At 21 h, DIRFA's ratio had decreased to 3.35, but dDIRFA remained stable with a ratio of 10.03 (Figure S7 21 h). These results demonstrate that the DNA-based aptamer (DIRFA) provides greater stability than the RNA-based broccoli aptamer, and that dimerization further enhances DIRFA's stability. Given its superior performance, we dimerized DASA sensors (dDASA) for intracellular applications.

Recognizing that Mg^{2+} ion concentrations can influence the fluorescence signals of fluorogenic aptamers,[86,87] we evaluated the behavior of the dDASA sensor in the presence and absence of Mg^{2+}. Our in test tube characterizations, conducted in PBS

https://doi.org/10.1021/jacs.4c09855
J. Am. Chem. Soc. 2025, 147, 1529−1541

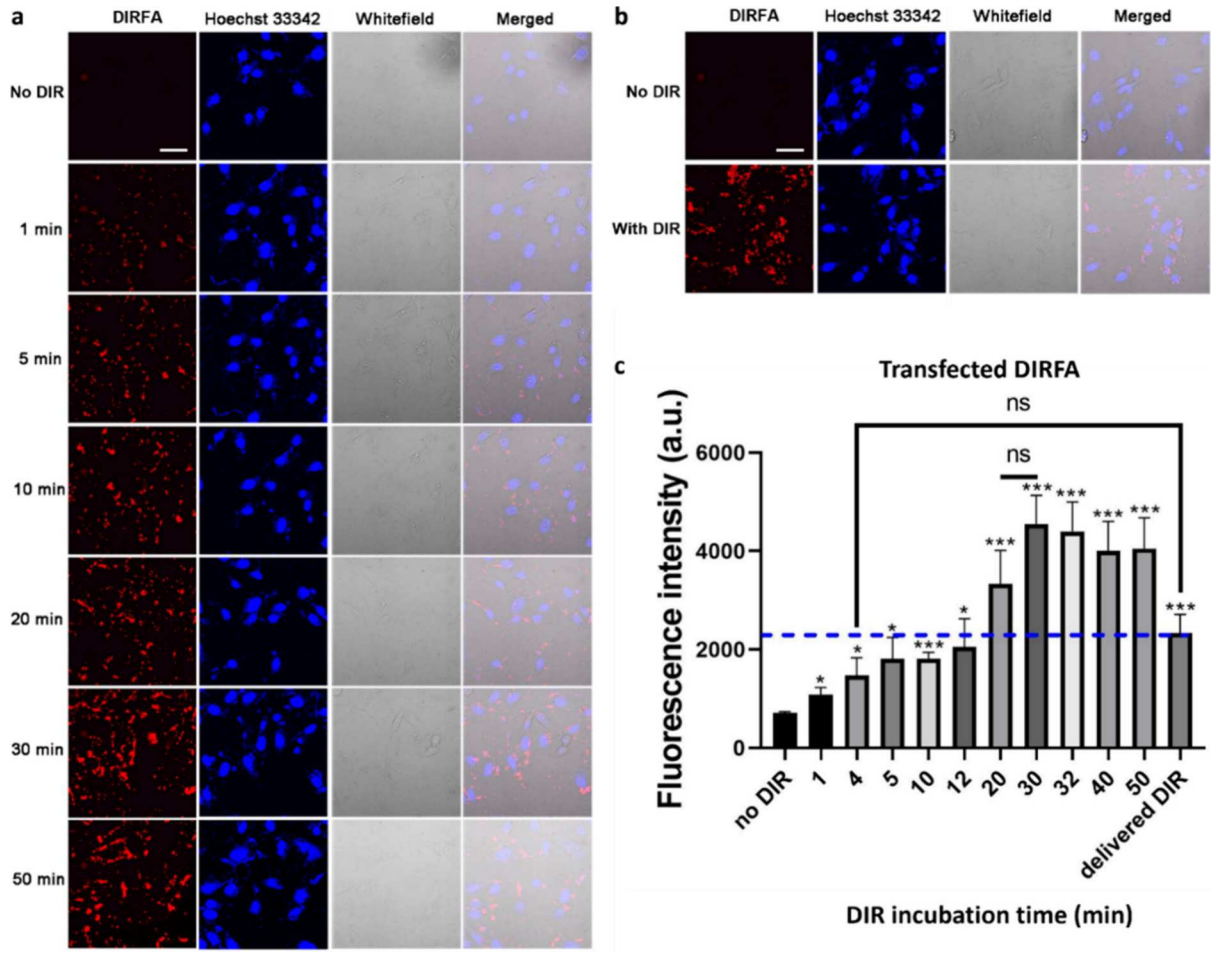

Figure 3. Assessment of Cell Membrane Permeability of DIR in HeLa Cells Using DIRFA. **a)** The DIRFA was delivered into HeLa cells without DIR. After the transfection and wash steps, DIR was then added to the cell culture media. The fluorescence of cells was recorded with a spinning disk confocal microscope at each time point during the DIR incubation. **b)** Images of the cells that were cotransfected with the same amount of DIRFA and DIR as used in a). The scale bars represent 50 μm. **c)** Quantification of the average fluorescence intensity in cells. The blue line indicates the mean fluorescence intensity of the cells when DIR was delivered together with the aptamer (right-most bar). The stars represent the results from student's t tests to compare the fluorescence intensity between different time points and the group without DIR treatments. ns, $p > 0.05$; *, $p < 0.05$; **, $p < 0.01$; ***, $p < 0.001$.

without additional Mg^{2+}, demonstrated that the sensing performance of dDASA is independent of Mg^{2+}, unlike some fluorogenic RNA aptamers.[88] While increasing Mg^{2+} concentrations at physiologically relevant levels caused minor fluctuations in overall fluorescence intensity (Figure S8a−b), the ratio of the 5 mM ATP signal to the background (without ATP) remained relatively stable (Figure S8c−d). These findings highlight the robustness of the dDASA sensor, making it well-suited for complex biological environments, such as cellular systems, where Mg^{2+} levels may vary. However, given that fluorescence intensity can be influenced by Mg^{2+} concentrations, it remains essential to include appropriate controls when analyzing small metabolite concentrations in such settings. These controls ensure accurate interpretation of results and enhance the sensor's reliability in practical applications.

To optimize the design of dDASA, we evaluated the dimers of DASA-1 to -4 (called dDASA-1 to -4 hereafter) by comparing their fluorescence spectra with and without ATP at either room temperature (22 °C) or 37 °C (Figure S9). When compared between Figure S5 and S9, the fluorescence intensity of the DASA sensors under both temperatures increased from 15% to a few folds after dimerization. In evaluating ATP sensing capabilities, dDASA-1 showed limited discrimination between ATP presence and absence at both temperatures. In contrast, dDASA-2 effectively distinguished ATP presence across both temperatures. While dDASA-3 produced a significant signal increase in the presence of ATP at room temperature, its response weakened at 37 °C, showing reduced signal strength and differentiation. Additionally, although dDASA-4 demonstrated strong fluorescence and differentiation in its monomeric form, its sensing ability diminished post dimerization. Based on the sensing performance of DASA monomers and dimers across both temperatures, dDASA-2 was selected for further investigation.

To evaluate if the length of the linker between monomers will influence the sensor performance, we tested 4-nt, 8-nt, 10-nt, and 13-nt linkers, and found that the 10-nt linker (dDASA 2-C) exhibited strong fluorescence and substantial fluorescence enhancement when detecting ATP in PBS buffer at both temperatures (Figure 2b−c and Figure S10−11). Therefore, we used dDASA 2-C for further experiments.

Introducing point mutations into the ATP aptamer to disrupt its binding affinity resulted in approximately 2-fold

https://doi.org/10.1021/jacs.4c09855
J. Am. Chem. Soc. 2025, 147, 1529−1541

lower fluorescence intensity in the mutated dDASA. The mutated aptamer exhibited a small but statistically insignificant fluorescence response upon ATP addition (Figure 2b−c, Figure S10). This small response could be attributed to the single-point mutation affecting only one binding site.[89] To evaluate the performance of the dDASA 2-C under both temperature conditions, we measured its detection range and observed nearly 2 orders of magnitude dynamic range (linear range between 0.05 and 2.5 mM of ATP at room temperature and 0.05−5 mM ATP at 37 °C, respectively, Figure 2d−e). Moreover, the dDASA 2-C sensor showed good selectivity over other rNTPs under both temperatures (Figure 2f−g).

We further evaluated the performance of both dimeric and monomeric forms of DASA sensors, specifically using the top-performing sequences dDASA 2-C and DASA-2 (hereafter referred to as dDASA and DASA, respectively), at room temperature through fluorescence microscopy.[90] We tested the performance of the probes under an excitation wavelength of 635 nm and an emission range of 685/40 nm, as these conditions are optimal for near-infrared fluorescent probes used in cellular imaging. This wavelength setup was selected to reduce phototoxicity and minimize spectral crosstalk with probes excitable by visible light. Additionally, these parameters were chosen to decrease scattering and absorption within mammalian tissues, thereby improving imaging clarity and accuracy.[91] Under these conditions, dDASA demonstrated a 155% increase in fluorescence intensity when sensing 5 mM ATP, compared to a 43% increase observed for DASA, further suggesting that dimerization enhanced the ATP sensing capability of the DASA sensor (Figure S12).

Temporal Control of ATP Sensing in Living Cells. After optimizing the dDASA sensor in test tubes, we transfected it into HeLa cells using the TurboFect transfection reagent and assessed its performance. The cells were then treated either with 5 mM $CaCl_2$ to increase intracellular ATP levels[75,92] or 10 μM oligomycin, an ATP synthase inhibitor,[93,94] to decrease ATP levels. Cells exposed to $CaCl_2$ exhibited higher fluorescence intensity, while those treated with oligomycin showed reduced intensity (Figure S13a−b). Introducing point mutations to disrupt the ATP binding pocket in dDASA (Mutated dDASA) resulted in displaying lower fluorescence intensity compared to the canonical dDASA (Figure S13a, c). More importantly, Mutated dDASA displayed minimal changes with $CaCl_2$ or oligomycin (Figure S13d), indicating that its fluorescence intensity variations were associated with ATP binding activity. We further confirmed the modulation of cellular ATP levels with these treatments using a Sigma adenosine 5′-triphosphate bioluminescent somatic cell assay kit (Figure S14). Hence, we concluded that dDASA could effectively sense ATP levels in living cells.

To evaluate the possibility of temporally controlled sensing, we evaluated how fast the sensor can respond to ATP or DIR by recording the fluorescence change with a fluorometer before and immediately after adding ATP or DIR. The fluorescence signal reached a plateau in <7s (Figure S15), the minimal handling and instrument response time that we were able to achieve with the fluorometer. This fast response suggests that the design has a potential for temporally controlled sensing. To evaluate if DIR can permeate cell membranes at a desired time point to initiate ATP sensing, we used DIRFA to assess how fast the aptamer displays observable fluorescent signals after incubating the DIR with cells. We delivered the DIRFA into HeLa cells and recorded the fluorescence signal of the cells with a microscope (Figure 3). The cell showed a 52% increase in fluorescence intensity as fast as being incubated with 1 μM DIR for 1 min. The fluorescence intensity increased over time and plateaued at 20 min, with no significant statistical differences observed beyond this point (Figure 3a, c).

For comparison, we cotransfected the same amount of DIRFA and DIR as used in the post-transfection incubation study. This cotransfection resulted in a fluorescence intensity comparable to that observed 4 min after the addition of DIR post-transfection (p = 0.1136, Figure 3b−c). However, this intensity was significantly lower than the plateau level observed after 30 min post-transfection incubation period (p = 0.0028, comparing the 30 min post-transfection incubation with the cotransfection of DIR). These findings suggest that DIR efficiently penetrates cells and enables rapid sensing within as little as 1 min, while a stabilized signal is achieved after 20−30 min of incubation.

Real-Time ATP Tracking in Living Cells. To assess whether the dDASA sensor can monitor ATP levels in real-time in living cells, we modulated intracellular ATP levels by alternating glucose concentrations in the cell culture media, given that glucose is a key energy source for ATP production.[95] After delivering the dDASA sensor into HeLa cells, we changed the concentration of glucose alternatively. A higher fluorescence signal was observed in cells cultured in high-glucose media (25 mM added glucose) and a reduced signal in cells exposed to glucose-free media (Figure 4a, c), indicating elevated ATP levels in high-glucose conditions and lower ATP levels in glucose-deprived conditions. These findings are consistent with previous studies[96] and corroborate results obtained from the ATP bioluminescent assay kit (Figure S14). To further validate these observations, we used dDASA to monitor ATP levels by alternately treating cells with 10 μM oligomycin and 5 mM $CaCl_2$. A decrease in fluorescence was observed with oligomycin treatment, indicating reduced ATP levels, while an increase in fluorescence followed $CaCl_2$ treatment, reflecting elevated ATP levels (Figure 4b, d). These results confirm that dDASA can reversibly track ATP levels in real-time. This also reinforces the conclusion that the fluorescence increase of the dDASA sensor upon ATP binding is reversible and can effectively reflect ATP dynamics in living cells.

Genetically Encoded Fluorogenic DNA Aptamer (GEFDA) Sensors for ATP Detection in Bacterial Cells. To expand the application of the DASA sensor, we transformed dDASA and its variant into DH10B bacterial cells and incubated them with DIR and 1 mM ATP. We noticed a marginal fluorescence increase in comparison to both ATP-absent condition (3.9%) and bacterial cells transformed with a mutated ATP aptamer (4.8%) (Figure S16), presumably due to the fast division of bacterial cells and subsequent dilution of the aptamer sensors. This observation is also consistent with previous reports that multiple copies of the RNA aptamers are necessary for imaging target molecules in *E. coli* cells.[97]

We hypothesized that consistently generating small-molecule sensors in bacterial cells would address the above issue. To synthesize dDASA in DH10B cells, we chose reverse transcriptase-based systems because, unlike the retron system,[98−100] it produces only the desired DNA without generating additional byproducts. We tested both a three-plasmid system[101] and a modified single-plasmid system adapted from Chen et al.[102−106] As a proof of concept, we

https://doi.org/10.1021/jacs.4c09855
J. Am. Chem. Soc. 2025, 147, 1529−1541

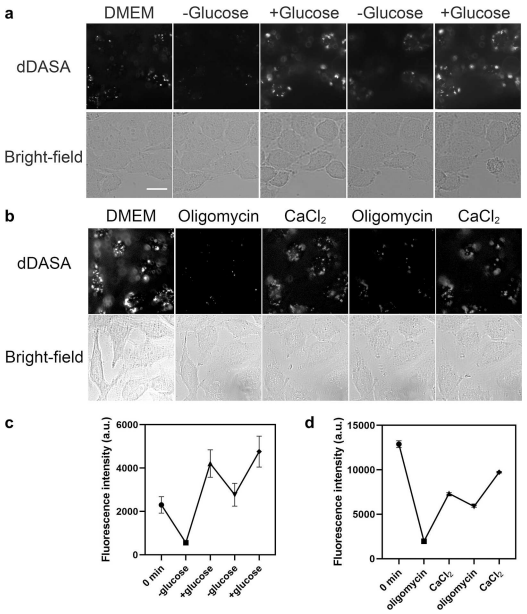

Figure 4. Real-Time ATP Tracking in HeLa Cells Using the dDASA Sensor. **a)** Cellular images demonstrated changes in ATP levels in response to varying glucose concentrations in the cell culture media. For the "-glucose" condition, cells were incubated in glucose-free DMEM for 1 h. In the "+glucose" condition, cells were cultured in DMEM containing 25 mM glucose for 1 h. Increased fluorescence signals were observed when treating the cells with glucose, while decreased fluorescence signals were observed when incubating the cells with glucose-free media. **b)** Cellular images revealed changes in ATP levels in response to treatments with 10 μM oligomycin and 5 mM $CaCl_2$. Fluorescence images were collected using a 640/15 nm excitation light and a 680/25 nm emission light immediately before the cells were transitioned to a new condition. Scale bars represent 20 μm. **c–d)** Statistical quantification of the average fluorescence intensity in cells for a) and b) respectively. The ATP levels were tracked in the same cell population.

tested the system with a 72-nt single-stranded DNA (ssDNA) but initially observed no DNA product (Figure S17 a, b). We hypothesized that the ssDNA might be rapidly degraded, as ssDNA binding proteins (SBPs) are critical for stabilizing single-stranded regions during replication or transcription.[107,108] To address this, we introduced the β protein to enhance ssDNA stability.[109−112] With the addition of β protein, distinct ssDNA bands became visible (Figure S17 b, c). To further enhance DNA yield, we constructed a high-copy plasmid, which led to a substantial increase in ssDNA production (Figure S17 d–e).

To assess the impact of SBP on the formation of the DIRFA/DIR complex, we tested two commercially available SBPs, ET SSB and Rec A. In the presence of SBP, the DIRFA/DIR complex exhibited a slight increase in fluorescence intensity compared to conditions lacking SBPs (Figure S17 f). This observation aligns with previous findings indicating that SBP can enhance aptamer functionality.[113−115] To evaluate if the plasmid can express functional GEFDA in bacterial cells, we replaced the 72-nt sequence with DIRFA or dDIRFA (GEFDA in the scheme in Figure 5a). The plasmid contains the following elements: 1) A rrnB T1 terminator for termination of transcription; 2) An IPTG inducible reverse transcriptase from Moloney mouse leukemia virus for reverse-transcription; 3) A val-tRNA binding sequence for initiation of reverse transcription (val-tRNA primer) in *E. coli*; 4) A hairpin structure for termination of reverse transcription; and 5) an IPTG inducible β. We transformed the plasmids into DH10B competent cells to express DIRFA or dDIRFA. The plasmids were transformed into DH10B cells and induced by IPTG. In DH10B cells transformed with the dDIRFA plasmid, over 40% displayed fluorescence levels above 10^3, while fluorescence at this level was nearly absent in the nontransformed control group (Figure 5b–c). This result confirms both the successful production and functional aptamer activity of dDIRFA in bacterial cells. When comparing dDIRFA with DIRFA, cells expressing the monomeric DIRFA showed only about 20% fluorescence-positive cells, suggesting that the dimeric form is likely brighter or more stable than the monomer in this cellular context (Figure S18).

To evaluate the sensing ability of the dDASA sensor as a GEFDA sensor, we replaced the DIRFA sequence in the plasmid with the dDASA sensor. After transformation, the bacterial cells were divided into three groups and incubated with either cell culture media alone, media supplemented with 50 μM ATP, or media containing 10 μM Venturicidin A (VentA), an ATP-synthase complex inhibitor that depletes intracellular ATP levels in bacterial cells.[116] Following treatment, the cells were incubated with DIR, and their fluorescence intensities were measured by flow cytometry. The results showed that DIR incubation produced only a minor increase in background fluorescence (Figure 5d, No DIR vs No IPTG), while IPTG induction significantly raised the fluorescence signal (Figure 5d, No IPTG vs Medium), indicating successful detection of intrinsic ATP levels in bacteria expressing the dDASA plasmid. Fluorescence intensity further increased in the bacteria incubated with 50 μM ATP (Figure 5d, Medium vs 50 μM ATP) and decreased in those treated with VentA (Figure 5d, Medium vs 10 μM VentA). These findings confirm that the dDASA plasmid can effectively detect intracellular ATP levels (Figure 5d, f).

Interestingly, two distinct bacterial subpopulations appeared under the "medium" condition (Figure 5d), suggesting that the sensor could differentiate subpopulations at single-cell resolution, offering insights into cellular responses to treatments. One subpopulation showed fluorescence similar to ATP-treated cells, while the other resembled VentA-treated cells, implying potential variability in ATP levels or sensor activity across the population. Although factors like transformation efficiency or expression variability may contribute to this distribution, the increase in fluorescence within the lower-intensity subpopulation upon ATP treatment suggests that the sensor was successfully delivered and synthesized in both subpopulations. This unique capability highlights the sensor's potential for resolving and monitoring ATP variability at single-cell resolution, offering valuable insights into cellular heterogeneity and response dynamics that warrant further investigation.

To confirm that the observed signal changes were specifically due to dDASA expression in response to intracellular ATP levels, we introduced point mutations into the ATP-binding site of dDASA and expressed the mutated version with the same system. Although adding DIR increased the baseline fluorescence of the mutated dDASA plasmid (Figure 5e, No DIR vs No IPTG), neither IPTG induction nor ATP level changes produced any additional fluorescence changes (Figure 5e, f). This suggests that the fluorescence intensity variations in the unmutated sensor were indeed due to ATP recognition and binding. Collectively, these results demon-

https://doi.org/10.1021/jacs.4c09855
J. Am. Chem. Soc. 2025, 147, 1529−1541

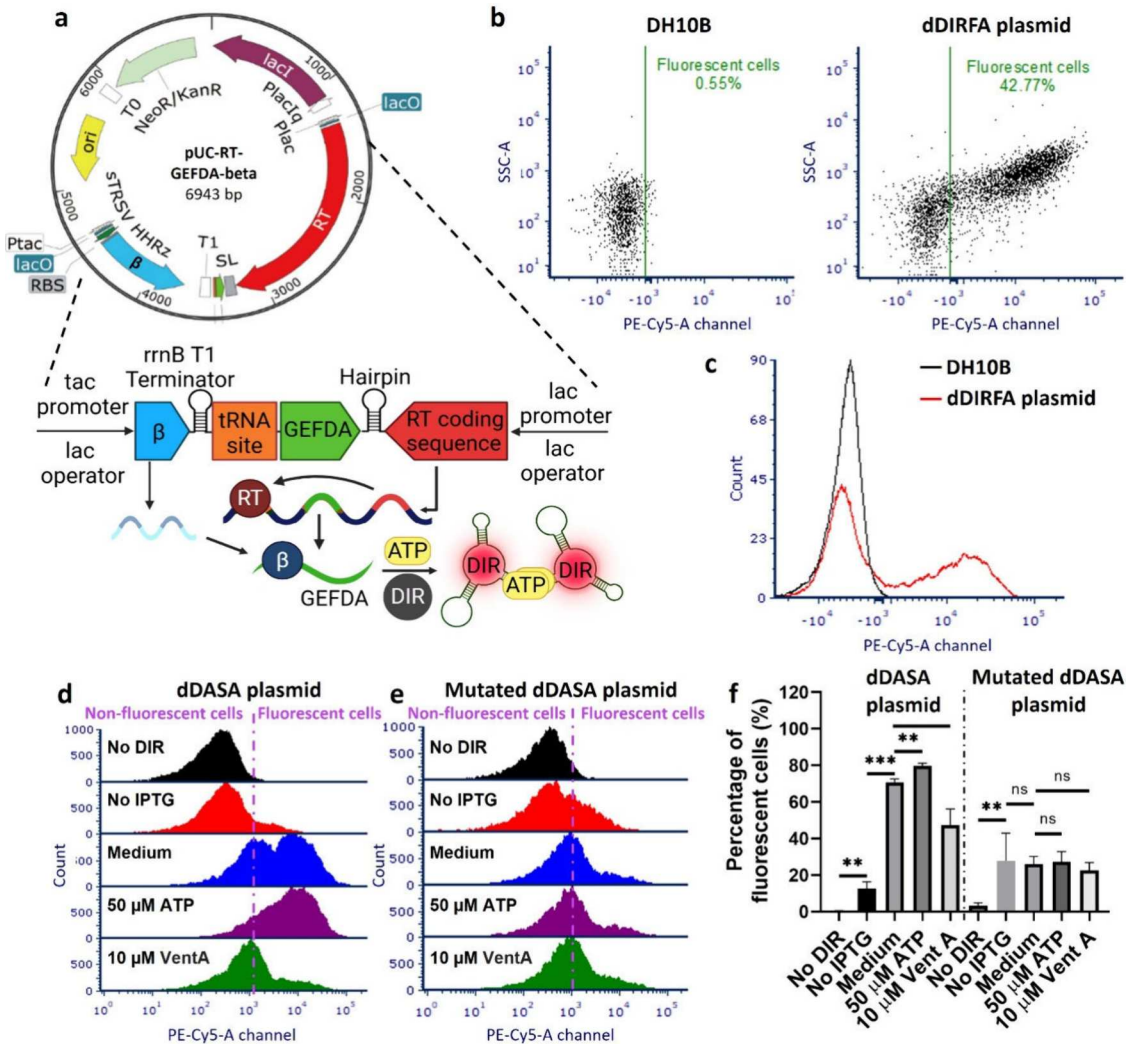

Figure 5. Genetically Encoded Fluorogenic DNA Aptamer (GEFDA) Sensor for Monitoring ATP Levels in *E. coli*. **a**) A scheme showed the major elements of the plasmid that generate GEFDA sensor in bacterial cells. The reverse transcriptase (RT) will be synthesized and bind to the tRNA binding site of the mRNA to initiate the reverse transcription of the GEFDA. With the help of β protein and the tandem repeat structure of the sensor, the plasmid has a higher yield for producing GEFDA in cells. **b**) The dot plot displayed the fluorescence intensity and size of individual DH10B cells as detected by flow cytometry analysis. More than 40% of the bacterial cells with the plasmid that codes dDIRFA showed higher fluorescence intensity than the cells without the plasmid. **c**) Histogram from flow cytometry showed the increase of fluorescence intensity in a population of the bacteria that expressed dDIRFA. **d**) Histogram from flow cytometry reflects that the genetically encoded dDASA monitored ATP levels in bacterial cells. The DH10B cells were transformed with the plasmids that express dDASA, and then incubated with IPTG and DIR. After the transfection and induction, the cells were divided into three groups, which were maintained in the cell culture media, or treated with 50 μM ATP or 10 μM Venturicidin A (VentA), respectively. Comparison was also made with the cells that were not induced by IPTG (No IPTG) or not incubated with DIR (No DIR) after the transformation. **e**) Histogram from flow cytometry reflects that the plasmid that expresses the Mutated dDASA was not able to monitor ATP levels. **f**) Statistical analysis for experiments in (e) and (f). The cells that showed a fluorescence intensity higher than 10^3 were considered fluorescent cells. The data were obtained from 7 independent experiments. ns, $p > 0.05$; *, $p < 0.05$; **, $p < 0.01$; ***, $p < 0.001$.

strate the successful development of GEFDA sensors capable of detecting ATP levels in bacterial cells.

GEFDA Sensors for Monitoring ATP in Mammalian Cells. To adapt the GEFDA sensor for ATP detection in mammalian cells, we cloned all essential components—inducible reverse transcriptase, T1 terminator, hairpin structure, val-tRNA binding sequence, and the β protein—into the pBK-CMV plasmid. This plasmid utilizes the CMV promoter to drive protein expression in mammalian cells, replacing the original plasmid backbone, which was driven by an *E. coli lac* promoter specific to prokaryotes.

To validate this system, we used dDIRFA to compare plasmid performance with and without the β protein. Following transfection with the plasmid expressing dDIRFA, cells showed increased fluorescence upon DIR incubation, whereas DIR incubation alone, without plasmid transfection, did not result in any fluorescence increase (Figure S19). Notably, the addition of β protein significantly enhanced fluorescence intensity (Figure S20). These experiments confirm the successful expression and functionality of dDIRFA in mammalian cells.

To assess the performance of the GEFDA sensor, we replaced dDIRFA with dDASA in the plasmid containing the β protein. After transfecting cells with this plasmid, we modulated cellular ATP levels using 10 μM oligomycin or 5 mM $CaCl_2$. Fluorescence intensity increased in cells treated

https://doi.org/10.1021/jacs.4c09855
J. Am. Chem. Soc. 2025, 147, 1529−1541

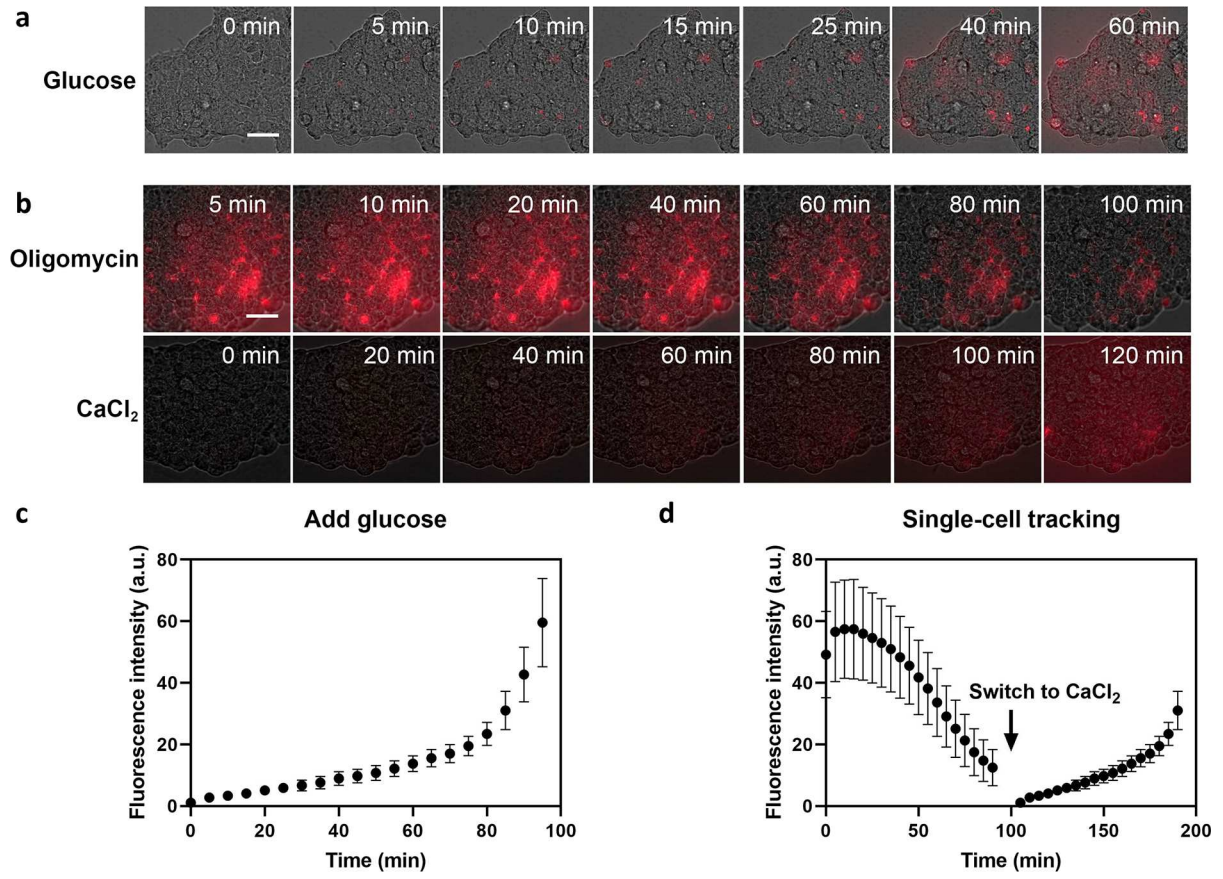

Figure 6. GEFDA Sensor for Monitoring ATP Levels in HeLa Cells. **a**) Cellular imaging was performed to sense ATP levels using the dDASA sensor expressed via a pBK-CMV plasmid. Single fields of cell populations were monitored while modulating ATP levels. Adding 25 mM glucose to cell culture media results in a gradual increase of fluorescence intensity, indicating the elevation of ATP levels. **b**) Single-field monitoring of ATP level changes when incubating cells with 10 μM oligomycin for 1.5 h followed. A slight initial increase in fluorescence intensity was observed, followed by a notable decline. Subsequent washing with PBS and the addition of cell culture media containing 5 mM $CaCl_2$ led to a gradual increase in fluorescence intensity. Scale bars: 40 μm. **c**) Statistical analysis of the cells in a). **d**) Statistical analysis for the cells in b).

with $CaCl_2$ and decreased in those treated with oligomycin. When the ATP-binding site was mutated, fluorescence intensity was no longer affected by these treatments (Figure S21). These experiments confirmed the successful ATP sensing capability of the GEFDA-dDASA sensor.

To evaluate whether the GEFDA-dDASA sensor can track real-time ATP dynamics in live cells, we monitored fluorescence changes in the same cell population while modulating intracellular ATP levels using 25 mM glucose, 10 μM oligomycin, or 5 mM $CaCl_2$. A gradual increase in fluorescence was observed during glucose incubation, confirming that our GEFDA sensor effectively tracks ATP levels in individual cells (Figure 6a, c, Movie S1). Interestingly, after the addition of 10 μM oligomycin, fluorescence initially increased before undergoing a marked decline (Figure 6b, d, Movie S2), aligning with previously reported compensatory glycolysis immediately following oligomycin treatment.[117] After replacing oligomycin with $CaCl_2$, the fluorescence intensity in the same cell population gradually recovered, suggesting that ATPase inhibition by oligomycin may be reversible (Figure 6b, d, Movie S3). These results confirm the successful detection and monitoring of intracellular ATP dynamics using the dDASA plasmid, highlighting its potential for future studies of cellular behavior through real-time event monitoring. To this end, we have demonstrated the potential of using GEFDA sensors to trace ATP levels in both bacterial and mammalian cells.

CONCLUSIONS

Although genetically encoded sensors based on fluorescent proteins and RNA aptamers have been widely used for visualizing cellular events, there is always a need for improved sensors to monitor metabolite concentrations in live cells. Taking advantage of the DNA aptamers which are more stable than RNA and can be easily reprogrammed, we developed a new genetically encoded fluorogenic DNA aptamer (GEFDA) sensor termed DASA for real-time detection of ATP in *E. coli* and HeLa cells. By overcoming the issues of all the prelabeled DNA aptamer sensors such as sensor dilution, degradation, and low S/B ratio in live-cell detection, our GEFDA-dDASA sensor expresses the dimeric sensor which contains dual chromophore binding sites and dual-target recognition sites with a plasmid that contains a tRNA binding sequence, terminators, and sequences that encode IPTG inducible reverse transcriptase and single-stranded DNA binding protein. With the GEFDA sensors, we monitored the ATP levels in both bacterial and mammalian cells. Utilizing the DNA aptamers allowed the expansion of the aptamer library from existing DNA aptamers and obtaining aptamers for new targets with SELEX. Therefore, this method signifies a major advancement in genetically encoded sensors by adding GEFDA as a new member, along with the fluorescent proteins and fluorogenic RNAs to detect small-molecule metabolites as valuable tools

https://doi.org/10.1021/jacs.4c09855
J. Am. Chem. Soc. 2025, 147, 1529−1541

for monitoring the real-time dynamics of metabolites and other small molecules in biological systems.

■ ASSOCIATED CONTENT

Supporting Information

The Supporting Information is available free of charge at https://pubs.acs.org/doi/10.1021/jacs.4c09855.

Experimental details and supplementary data, including optimization of DNA sequences, characterization of DASA and dDASA fluorogenic aptamer sensors, utilizing dDASA sensors for imaging ATP levels in mammalian cells, flow cytometry assay of bacterial cells, express DIRFA in mammalian cells. Table of DNA sequences (PDF)

Movie S1: GEFDA Sensor Monitoring ATP Levels in Live HeLa Cells After 25 mM Glucose Addition (AVI)

Movie S2: GEFDA Sensor Monitoring ATP Levels in Live HeLa Cells After 10 μM Oligomycin Addition (AVI)

Movie S3: Fluorescence Recovery After Treatment Removal and 5 mM $CaCl_2$ Addition in Cells from Movie S2 (AVI)

■ AUTHOR INFORMATION

Corresponding Author

Yi Lu − *Department of Chemistry, The University of Texas at Austin, Austin, Texas 78712, United States; Department of Chemistry, University of Illinois at Urbana−Champaign, Urbana, Illinois 61801, United States; Department of Molecular Biosciences, The University of Texas at Austin, Austin, Texas 78712, United States; Department of Biochemistry, University of Illinois at Urbana−Champaign, Urbana, Illinois 61801, United States;* orcid.org/0000-0003-1221-6709; Email: yi.lu@utexas.edu

Authors

Yuting Wu − *Department of Chemistry, The University of Texas at Austin, Austin, Texas 78712, United States; Department of Chemistry, University of Illinois at Urbana−Champaign, Urbana, Illinois 61801, United States;* orcid.org/0000-0003-3196-5916

Wentao Kong − *Department of Bioengineering, University of Illinois at Urbana−Champaign, Urbana, Illinois 61801, United States*

Jacqueline Van Stappen − *Department of Chemistry, The University of Texas at Austin, Austin, Texas 78712, United States*

Linggen Kong − *Department of Molecular Biosciences and Interdisciplinary Life Sciences Graduate Programs, The University of Texas at Austin, Austin, Texas 78712, United States*

Zhimei Huang − *Department of Chemistry, University of Illinois at Urbana−Champaign, Urbana, Illinois 61801, United States*

Zhenglin Yang − *Department of Chemistry, The University of Texas at Austin, Austin, Texas 78712, United States; Department of Biochemistry, University of Illinois at Urbana−Champaign, Urbana, Illinois 61801, United States*

Yu-An Kuo − *Department of Biomedical Engineering, The University of Texas at Austin, Austin, Texas 78712, United States*

Yuan-I Chen − *Department of Biomedical Engineering, The University of Texas at Austin, Austin, Texas 78712, United States;* orcid.org/0000-0002-9559-2779

Yujie He − *Department of Biomedical Engineering, The University of Texas at Austin, Austin, Texas 78712, United States;* orcid.org/0000-0002-6984-3052

Hsin-Chih Yeh − *Department of Biomedical Engineering and Texas Materials Institute, The University of Texas at Austin, Austin, Texas 78712, United States;* orcid.org/0000-0001-6654-5626

Ting Lu − *Department of Bioengineering and Center for Advanced Bioenergy and Bioproducts Innovation, University of Illinois at Urbana−Champaign, Urbana, Illinois 61801, United States;* orcid.org/0000-0001-9043-3253

Complete contact information is available at: https://pubs.acs.org/10.1021/jacs.4c09855

Notes

The authors declare the following competing financial interest(s): Y.L., Y.W., W.K., T. L., J.V.S., and L.K are inventors on U.S. Patent Application No. 63/667,359, filed by the University of Texas System, which covers the contents of this article.

■ ACKNOWLEDGMENTS

This material is based on work supported by the US National Institute of Health (GM141931 to Y.L.) and the US National Science Foundation (CBET2235455 to H.-C.Y. and Y.L.). The Lu group research is supported by the Robert A. Welch Foundation (grant F-0020). W.K. and T.L. were supported by the DOE Center for Advanced Bioenergy and Bioproducts Innovation (U.S. Department of Energy, Office of Science, Office of Biological and Environmental Research under Award Number DE-SC0018420). H.-C.Y. was supported by the National Science Foundation (CHE2404334) and the National Institutes of Health (DA060543).

■ REFERENCES

(1) Greenwald, E. C.; Mehta, S.; Zhang, J. Genetically Encoded Fluorescent Biosensors Illuminate the Spatiotemporal Regulation of Signaling Networks. *Chem. Rev.* **2018**, *118* (24), 11707−11794.

(2) Kim, H.; Ju, J.; Lee, H. N.; Chun, H.; Seong, J. Genetically Encoded Biosensors Based on Fluorescent Proteins. *Sensors* **2021**, *21* (3), 795.

(3) Ovechkina, V. S.; Zakian, S. M.; Medvedev, S. P.; Valetdinova, K. R. Genetically Encoded Fluorescent Biosensors for Biomedical Applications. *Biomedicines* **2021**, *9* (11), 1528.

(4) Imamura, H.; Huynh Nhat, K. P.; Togawa, H.; Saito, K.; Iino, R.; Kato-Yamada, Y.; Nagai, T.; Noji, H. Visualization of ATP Levels inside Single Living Cells with Fluorescence Resonance Energy Transfer-Based Genetically Encoded Indicators. *Proc. Natl. Acad. Sci. U. S. A.* **2009**, *106* (37), 15651−15656.

(5) Yaginuma, H.; Kawai, S.; Tabata, K. V.; Tomiyama, K.; Kakizuka, A.; Komatsuzaki, T.; Noji, H.; Imamura, H. Diversity in ATP Concentrations in a Single Bacterial Cell Population Revealed by Quantitative Single-Cell Imaging. *Sci. Rep.* **2014**, *4*, 6522.

(6) Lobas, M. A.; Tao, R.; Nagai, J.; Kronschläger, M. T.; Borden, P. M.; Marvin, J. S.; Looger, L. L.; Khakh, B. S. A Genetically Encoded Single-Wavelength Sensor for Imaging Cytosolic and Cell Surface ATP. *Nat. Commun.* **2019**, *10*, 711.

(7) Leonard, A. C.; Whitehead, T. A. Design and Engineering of Genetically Encoded Protein Biosensors for Small Molecules. *Curr. Opin. Biotechnol.* **2022**, *78*, 102787.

(8) Mishra, K.; Fuenzalida-Werner, J. P.; Pennacchietti, F.; Janowski, R.; Chmyrov, A.; Huang, Y.; Zakian, C.; Klemm, U.; Testa, I.;

Niessing, D.; Ntziachristos, V.; Stiel, A. C. Genetically Encoded Photo-Switchable Molecular Sensors for Optoacoustic and Super-Resolution Imaging. *Nat. Biotechnol.* **2022**, *40* (4), 598−605.
(9) Park, J.; Cleary, M. B.; Li, D.; Mattocks, J. A.; Xu, J.; Wang, H.; Mukhopadhyay, S.; Gale, E. M.; Cotruvo, J. A. A Genetically Encoded Fluorescent Sensor for Manganese(II), Engineered from Lanmodulin. *Proc. Natl. Acad. Sci. U. S. A.* **2022**, *119* (51), No. e2212723119.
(10) Chen, Y.; Pang, S.; Li, J.; Lu, Y.; Gao, C.; Xiao, Y.; Chen, M.; Wang, M.; Ren, X. Genetically Encoded Protein Sensors for Metal Ion Detection in Biological Systems: A Review and Bibliometric Analysis. *Analyst* **2023**, *148* (22), 5564−5581.
(11) Xiong, M.; Yang, Z.; Lake, R. J.; Li, J.; Hong, S.; Fan, H.; Zhang, X.-B.; Lu, Y. DNAzyme-Mediated Genetically Encoded Sensors for Ratiometric Imaging of Metal Ions in Living Cells. *Angew Chem Int Ed* **2020**, *59* (5), 1891−1896.
(12) Meyer, A.; Pellaux, R.; Potot, S.; Becker, K.; Hohmann, H.-P.; Panke, S.; Held, M. Optimization of a Whole-Cell Biocatalyst by Employing Genetically Encoded Product Sensors inside Nanolitre Reactors. *Nat. Chem.* **2015**, *7* (8), 673−678.
(13) Xiao, Y.; Jiang, W.; Zhang, F. Developing a Genetically Encoded, Cross-Species Biosensor for Detecting Ammonium and Regulating Biosynthesis of Cyanophycin. *ACS Synth. Biol.* **2017**, *6* (10), 1807−1815.
(14) Ibraheem, A.; Yap, H.; Ding, Y.; Campbell, R. E. A Bacteria Colony-Based Screen for Optimal Linker Combinations in Genetically Encoded Biosensors. *BMC Biotechnol.* **2011**, *11* (1), 105.
(15) Chaisupa, P.; Wright, R. C. State-of-the-Art in Engineering Small Molecule Biosensors and Their Applications in Metabolic Engineering. *SLAS Technol.* **2024**, *29* (2), 100113.
(16) Frei, M. S.; Mehta, S.; Zhang, J. Next-Generation Genetically Encoded Fluorescent Biosensors Illuminate Cell Signaling and Metabolism. *Annu Rev Biophys* . **2024**, *53*, 275.
(17) Fowler, C. C.; Li, Y. Construction and Application of Riboswitch-Based Sensors That Detect Metabolites Within Bacterial Cells. In *Therapeutic Applications of Ribozymes and Riboswitches: Methods and Protocols*; Lafontaine, D.; Dubé, A., Eds.; Humana Press: Totowa, NJ, 2014; pp 177−197.
(18) Litke, J. L.; You, M.; Jaffrey, S. R. Developing Fluorogenic Riboswitches for Imaging Metabolite Concentration Dynamics in Bacterial Cells. *Methods Enzymol.* **2016**, *572*, 315−333.
(19) Kim, H.; Jaffrey, S. R. A Fluorogenic RNA-Based Sensor Activated by Metabolite-Induced RNA Dimerization. *Cell Chem. Biol.* **2019**, *26* (12), 1725−1731.
(20) Karunanayake Mudiyanselage, A. P. K. K.; Wu, R.; Leon-Duque, M. A.; Ren, K.; You, M. Second-Generation" Fluorogenic RNA-Based Sensors. *Methods* **2019**, *161*, 24−34.
(21) Wu, R.; Karunanayake Mudiyanselage, A. P. K. K.; Ren, K.; Sun, Z.; Tian, Q.; Zhao, B.; Bagheri, Y.; Lutati, D.; Keshri, P.; You, M. Ratiometric Fluorogenic RNA-Based Sensors for Imaging Live-Cell Dynamics of Small Molecules. *ACS Appl. Bio Mater.* **2020**, *3* (5), 2633−2642.
(22) Su, Y.; Hammond, M. C. RNA-Based Fluorescent Biosensors for Live Cell Imaging of Small Molecules and RNAs. *Curr. Opin. Biotechnol.* **2020**, *63*, 157−166.
(23) Shafiei, F.; McAuliffe, K.; Bagheri, Y.; Sun, Z.; Yu, Q.; Wu, R.; You, M. Paper-Based Fluorogenic RNA Aptamer Sensors for Label-Free Detection of Small Molecules. *Anal. Methods* **2020**, *12* (21), 2674−2681.
(24) Swetha, P.; Fan, Z.; Wang, F.; Jiang, J.-H. Genetically Encoded Light-up RNA Aptamers and Their Applications for Imaging and Biosensing. *J. Mater. Chem. B* **2020**, *8* (16), 3382−3392.
(25) Yu, Q.; Ren, K.; You, M. Genetically Encoded RNA Nanodevices for Cellular Imaging and Regulation. *Nanoscale* **2021**, *13* (17), 7988−8003.
(26) Sun, Z.; Wu, R.; Zhao, B.; Zeinert, R.; Chien, P.; You, M. Live-Cell Imaging of Guanosine Tetra- and Pentaphosphate (p)ppGpp with RNA-Based Fluorescent Sensors**. *Angew. Chem., Int. Ed.* **2021**, *60* (45), 24070−24074.
(27) Zheng, G.; Zhao, L.; Yuan, D.; Li, J.; Yang, G.; Song, D.; Miao, H.; Shu, L.; Mo, X.; Xu, X.; Li, L.; Song, X.; Zhao, Y. A Genetically Encoded Fluorescent Biosensor for Monitoring ATP in Living Cells with Heterobifunctional Aptamers. *Biosens. Bioelectron.* **2022**, *198*, 113827.
(28) Chen, Z.; Chen, W.; Reheman, Z.; Jiang, H.; Wu, J.; Li, X. Genetically Encoded RNA-Based Sensors with Pepper Fluorogenic Aptamer. *Nucleic Acids Res.* **2023**, *51* (16), 8322−8336.
(29) Fan, Z.; Dou, C.-X.; Tang, L.-J.; Wang, F.; Jiang, J.-H. Genetically Encoded RNA Sensors for Ratiometric and Multiplexed Imaging of Small Molecules in Living Cells. *Anal. Chem.* **2023**, *95* (38), 14455−14464.
(30) Mi, L.; Yu, Q.; Karunanayake Mudiyanselage, A. P. K. K.; Wu, R.; Sun, Z.; Zheng, R.; Ren, K.; You, M. Genetically Encoded RNA-Based Bioluminescence Resonance Energy Transfer (BRET) Sensors. *ACS Sens.* **2023**, *8* (1), 308−316.
(31) You, M.; Litke, J. L.; Jaffrey, S. R. Imaging Metabolite Dynamics in Living Cells Using a Spinach-Based Riboswitch. *Proc. Natl. Acad. Sci. U. S. A.* **2015**, *112* (21), No. E2756-E2765.
(32) Filonov, G. S.; Kam, C. W.; Song, W.; Jaffrey, S. R. In-Gel Imaging of RNA Processing Using Broccoli Reveals Optimal Aptamer Expression Strategies. *Chem. Biol.* **2015**, *22* (5), 649−660.
(33) Litke, J. L.; Jaffrey, S. R. Highly Efficient Expression of Circular RNA Aptamers in Cells Using Autocatalytic Transcripts. *Nat. Biotechnol.* **2019**, *37* (6), 667−675.
(34) Li, Y. A Quarter Century of In Vitro Selection. *J. Mol. Evol.* **2015**, *81* (5), 137−139.
(35) Ellington, A. D.; Szostak, J. W. Selection in Vitro of Single-Stranded DNA Molecules That Fold into Specific Ligand-Binding Structures. *Nature* **1992**, *355* (6363), 850−852.
(36) Peinetti, A. S.; Lake, R. J.; Cong, W.; Cooper, L.; Wu, Y.; Ma, Y.; Pawel, G. T.; Toimil-Molares, M. E.; Trautmann, C.; Rong, L.; Mariñas, B.; Azzaroni, O.; Lu, Y. Direct Detection of Human Adenovirus or SARS-CoV-2 with Ability to Inform Infectivity Using DNA Aptamer-Nanopore Sensors. *Sci. Adv.* **2021**, *7* (39), No. eabh2848.
(37) Mou, Q.; Xue, X.; Ma, Y.; Banik, M.; Garcia, V.; Guo, W.; Wang, J.; Song, T.; Chen, L.-Q.; Lu, Y. Efficient Delivery of a DNA Aptamer-Based Biosensor into Plant Cells for Glucose Sensing through Thiol-Mediated Uptake. *Sci. Adv.* **2022**, *8* (26), No. eabo0902.
(38) Hong, S.; Yang, Z.; Mou, Q.; Luan, Y.; Zhang, B.; Pei, R.; Lu, Y. Monitoring Leaching of Cd2+ from Cadmium-Based Quantum Dots by an Cd Aptamer Fluorescence Sensor. *Biosens. Bioelectron.* **2023**, *220*, 114880.
(39) Ma, Y.; Guo, W.; Mou, Q.; Shao, X.; Lyu, M.; Garcia, V.; Kong, L.; Lewis, W.; Ward, C.; Yang, Z.; Pan, X.; Yi, S. S.; Lu, Y. Spatial Imaging of glycoRNA in Single Cells with ARPLA. *Nat. Biotechnol.* **2024**, *42* (4), 608−616.
(40) Murakami, K.; Izuo, N.; Bitan, G. Aptamers Targeting Amyloidogenic Proteins and Their Emerging Role in Neurodegenerative Diseases. *J. Biol. Chem.* **2022**, *298* (1), 101478.
(41) Yang, L. F.; Ling, M.; Kacherovsky, N.; Pun, S. H. Aptamers 101: Aptamer Discovery and in Vitro Applications in Biosensors and Separations. *Chem. Sci.* **2023**, *14* (19), 4961−4978.
(42) Nutiu, R.; Li, Y. Structure-Switching Signaling Aptamers: Transducing Molecular Recognition into Fluorescence Signaling. *Chem.- Eur. J.* **2004**, *10* (8), 1868−1876.
(43) Xiao, Y.; Lubin, A. A.; Heeger, A. J.; Plaxco, K. W. Label-Free Electronic Detection of Thrombin in Blood Serum by Using an Aptamer-Based Sensor. *Angew. Chem., Int. Ed.* **2005**, *44* (34), 5456.
(44) Navani, N. K.; Li, Y. Nucleic Acid Aptamers and Enzymes as Sensors. *Curr. Opin. Chem. Biol.* **2006**, *10*, 272−281.
(45) Roncancio, D.; Yu, H.; Xu, X.; Wu, S.; Liu, R.; Debord, J.; Lou, X.; Xiao, Y. A Label-Free Aptamer-Fluorophore Assembly for Rapid and Specific Detection of Cocaine in Biofluids. *Anal. Chem.* **2014**, *86* (22), 11100−11106.
(46) Chen, T.-T.; Tian, X.; Liu, C.-L.; Ge, J.; Chu, X.; Li, Y. Fluorescence Activation Imaging of Cytochrome c Released from

https://doi.org/10.1021/jacs.4c09855
J. Am. Chem. Soc. 2025, 147, 1529−1541

Mitochondria Using Aptameric Nanosensor. *J. Am. Chem. Soc.* **2015**, *137* (2), 982−989.
(47) Pfeiffer, F.; Mayer, G. Selection and Biosensor Application of Aptamers for Small Molecules. *Front. Chem.* **2016**, *4*, 00025.
(48) Alkhamis, O.; Yang, W.; Farhana, R.; Yu, H.; Xiao, Y. Label-Free Profiling of DNA Aptamer-Small Molecule Binding Using T5 Exonuclease. *Nucleic Acids Res.* **2020**, *48* (20), No. e120.
(49) Wu, Y.; Yang, Z.; Lu, Y. Photocaged Functional Nucleic Acids for Spatiotemporal Imaging in Biology. *Curr. Opin. Chem. Biol.* **2020**, *57*, 95−104.
(50) Upan, J.; Youngvises, N.; Tuantranont, A.; Karuwan, C.; Banet, P.; Aubert, P.-H.; Jakmunee, J. A Simple Label-Free Electrochemical Sensor for Sensitive Detection of Alpha-Fetoprotein Based on Specific Aptamer Immobilized Platinum Nanoparticles/Carboxylated-Graphene Oxide. *Sci. Rep.* **2021**, *11* (1), 13969.
(51) Hong, S.; Pawel, G. T.; Pei, R.; Lu, Y. Recent Progress in Developing Fluorescent Probes for Imaging Cell Metabolites. *Biomed. Mater.* **2021**, *16* (4), 044108.
(52) Yu, H.; Alkhamis, O.; Canoura, J.; Liu, Y.; Xiao, Y. Advances and Challenges in Small-Molecule DNA Aptamer Isolation, Characterization, and Sensor Development. *Angew. Chem., Int. Ed.* **2021**, *60* (31), 16800−16823.
(53) Li, N.; Wang, X.; Tibbs, J.; Che, C.; Peinetti, A. S.; Zhao, B.; Liu, L.; Barya, P.; Cooper, L.; Rong, L.; Wang, X.; Lu, Y.; Cunningham, B. T. Label-Free Digital Detection of Intact Virions by Enhanced Scattering Microscopy. *J. Am. Chem. Soc.* **2022**, *144* (4), 1498−1502.
(54) Zhang, J.; Lan, T.; Lu, Y. Overcoming Major Barriers to Developing Successful Sensors for Practical Applications Using Functional Nucleic Acids. *Annu. Rev. Anal. Chem.* **2022**, *15* (1), 151−171.
(55) Chingarande, R. G.; Tian, K.; Kuang, Y.; Sarangee, A.; Hou, C.; Ma, E.; Ren, J.; Hawkins, S.; Kim, J.; Adelstein, R.; Chen, S.; Gillis, K. D.; Gu, L.-Q. Real-Time Label-Free Detection of Dynamic Aptamer-Small Molecule Interactions Using a Nanopore Nucleic Acid Conformational Sensor. *Proc. Natl. Acad. Sci. U. S. A.* **2023**, *120* (24), No. e2108118120.
(56) Zhang, S.; Song, G.; Yang, Z.; Kang, K.; Liu, X. A Label-Free Fluorescence Aptamer Sensor for Point-of-Care Serotonin Detection. *Talanta* **2024**, *277*, 126363.
(57) Gu, L.; Zhang, Y.; Wang, D.; Liu, J. Light-Up Sensing Citrate Using a Capture-Selected DNA Aptamer. *Adv. Sens. Res.* **2024**, *3* (6), 2300167.
(58) Xu, W. C.; Lu, Y. Label-Free Fluorescent Aptamer Sensor Based on Regulation of Malachite Green Fluorescence. *Anal. Chem.* **2010**, *82* (2), 574−578.
(59) Wang, H.; Wang, J.; Sun, N.; Cheng, H.; Chen, H.; Pei, R. Selection and Characterization of Malachite Green Aptamers for the Development of Light-up Probes. *ChemistrySelect* **2016**, *1* (8), 1571−1574.
(60) Kato, T.; Shimada, I.; Kimura, R.; Hyuga, M. Light-up Fluorophore-DNA Aptamer Pair for Label-Free Turn-on Aptamer Sensors. *Chem. Commun.* **2016**, *52* (21), 4041−4044.
(61) Chen, Y.; Wang, J.; Zhang, Y.; Xu, L.; Gao, T.; Wang, B.; Pei, R. Selection and Characterization of a DNA Aptamer to Crystal Violet. *Photochem. Photobiol. Sci.* **2018**, *17* (6), 800−806.
(62) Sando, S.; Narita, A.; Aoyama, Y. Light-up Hoechst-DNA Aptamer Pair: Generation of an Aptamer-Selective Fluorophore from a Conventional DNA-Staining Dye. *Chembiochem Eur. J. Chem. Biol.* **2007**, *8* (15), 1795−1803.
(63) Song, G.; Zou, Z.; Feng, A.; Li, C.; Liang, M.; Wang, F.; Liu, X. Light-Up Aptameric Sensor of Serotonin for Point-of-Care Use. *Anal. Chem.* **2023**, *95* (23), 9076−9082.
(64) VarnBuhler, B. S.; Moon, J.; Dey, S. K.; Wu, J.; Jaffrey, S. R. Detection of SARS-CoV-2 RNA Using a DNA Aptamer Mimic of Green Fluorescent Protein. *ACS Chem. Biol.* **2022**, *17* (4), 840−853.
(65) Ouellet, J. RNA Fluorescence with Light-Up Aptamers. *Front. Chem.* **2016**, *4*, 0029.
(66) Filonov, G. S.; Moon, J. D.; Svensen, N.; Jaffrey, S. R. Broccoli: Rapid Selection of an RNA Mimic of Green Fluorescent Protein by Fluorescence-Based Selection and Directed Evolution. *J. Am. Chem. Soc.* **2014**, *136* (46), 16299−16308.
(67) Tan, X.; Constantin, T. P.; Sloane, K. L.; Waggoner, A. S.; Bruchez, M. P.; Armitage, B. A. Fluoromodules Consisting of a Promiscuous RNA Aptamer and Red or Blue Fluorogenic Cyanine Dyes: Selection, Characterization, and Bioimaging. *J. Am. Chem. Soc.* **2017**, *139* (26), 9001−9009.
(68) Bai, J.; Luo, Y.; Wang, X.; Li, S.; Luo, M.; Yin, M.; Zuo, Y.; Li, G.; Yao, J.; Yang, H.; Zhang, M.; Wei, W.; Wang, M.; Wang, R.; Fan, C.; Zhao, Y. A Protein-Independent Fluorescent RNA Aptamer Reporter System for Plant Genetic Engineering. *Nat. Commun.* **2020**, *11*, 3847.
(69) Vibhute, M. A.; Machatzke, C.; Bigler, K.; Krümpel, S.; Summerer, D.; Mutschler, H. Intracellular Expression of a Fluorogenic DNA Aptamer Using Retron Eco2. *eLife* **2024**, *13*, 99554.
(70) Karunanayake Mudiyanselage, A. P. K. K.; Wu, R.; Leon-Duque, M. A.; Ren, K.; You, M. "Second-generation" fluorogenic RNA-based sensors. *Methods* **2019**, *161*, 24−34.
(71) Wang, H.; Wang, J.; Wang, Q.; Chen, X.; Liu, M.; Chen, H.; Pei, R. Selection and Characterization of Dimethylindole Red DNA Aptamers for the Development of Light-up Fluorescent Probes. *Talanta* **2017**, *168*, 217−221.
(72) Huizenga, D. E.; Szostak, J. W. A DNA Aptamer That Binds Adenosine and ATP. *Biochemistry* **1995**, *34* (2), 656−665.
(73) Liu, Z.; Chen, S.; Liu, B.; Wu, J.; Zhou, Y.; He, L.; Ding, J.; Liu, J. Intracellular Detection of ATP Using an Aptamer Beacon Covalently Linked to Graphene Oxide Resisting Nonspecific Probe Displacement. *Anal. Chem.* **2014**, *86* (24), 12229−12235.
(74) Zhao, J.; Gao, J.; Xue, W.; Di, Z.; Xing, H.; Lu, Y.; Li, L. Upconversion Luminescence-Activated DNA Nanodevice for ATP Sensing in Living Cells. *J. Am. Chem. Soc.* **2018**, *140* (2), 578−581.
(75) Hong, S.; Zhang, X. J.; Lake, R. T.; Pawel, G.; Guo, Z.; Pei, R.; Lu, Y. A Photo-Regulated Aptamer Sensor for Spatiotemporally Controlled Monitoring of ATP in the Mitochondria of Living Cells. *Chem. Sci.* **2020**, *11* (3), 713−720.
(76) Xiong, Y.; Zhang, J.; Yang, Z.; Mou, Q.; Ma, Y.; Xiong, Y.; Lu, Y. Functional DNA Regulated CRISPR-Cas12a Sensors for Point-of-Care Diagnostics of Non-Nucleic-Acid Targets. *J. Am. Chem. Soc.* **2020**, *142* (1), 207−213.
(77) Banik, M.; Ledray, A. P.; Wu, Y.; Lu, Y. Delivering DNA Aptamers Across the Blood-Brain Barrier Reveals Heterogeneous Decreased ATP in Different Brain Regions of Alzheimer's Disease Mouse Models. *ACS Cent. Sci.* **2024**, *10*, 1585.
(78) Zhou, C.; Yu, Z.; Yu, W.; Liu, H.; Zhang, H.; Guo, C. Split Aptamer-Based Detection of Adenosine Triphosphate Using Surface Enhanced Raman Spectroscopy and Two Kinds of Gold Nanoparticles. *Microchim. Acta* **2019**, *186* (4), 251.
(79) Debiais, M.; Lelievre, A.; Smietana, M.; Müller, S. Splitting Aptamers and Nucleic Acid Enzymes for the Development of Advanced Biosensors. *Nucleic Acids Res.* **2020**, *48* (7), 3400−3422.
(80) Zhao, Y.; Patel, N.; Sun, P.; Faulds, K.; Graham, D.; Liu, J. Light-up Split Aptamers: Binding Thermodynamics and Kinetics for Sensing. *Analyst* **2023**, *148* (22), 5612−5618.
(81) Hasegawa, H.; Taira, K.; Sode, K.; Ikebukuro, K. Improvement of Aptamer Affinity by Dimerization. *Sensors* **2008**, *8* (2), 1090−1098.
(82) Bouhedda, F.; Fam, K. T.; Collot, M.; Autour, A.; Marzi, S.; Klymchenko, A.; Ryckelynck, M. A Dimerization-Based Fluorogenic Dye-Aptamer Module for RNA Imaging in Live Cells. *Nat. Chem. Biol.* **2020**, *16* (1), 69−76.
(83) Ueki, R.; Uchida, S.; Kanda, N.; Yamada, N.; Ueki, A.; Akiyama, M.; Toh, K.; Cabral, H.; Sando, S. A Chemically Unmodified Agonistic DNA with Growth Factor Functionality for in Vivo Therapeutic Application. *Sci. Adv.* **2020**, *6* (14), No. eaay2801.
(84) Riccardi, C.; Napolitano, E.; Musumeci, D.; Montesarchio, D. Dimeric and Multimeric DNA Aptamers for Highly Effective Protein Recognition. *Molecules* **2020**, *25* (22), 5227.

https://doi.org/10.1021/jacs.4c09855
J. Am. Chem. Soc. 2025, 147, 1529−1541

(85) Zhang, Z.; Pandey, R.; Li, J.; Gu, J.; White, D.; Stacey, H. D.; Ang, J. C.; Steinberg, C.-J.; Capretta, A.; Filipe, C. D. M.; Mossman, K.; Balion, C.; Miller, M. S.; Salena, B. J.; Yamamura, D.; Soleymani, L.; Brennan, J. D.; Li, Y. High-Affinity Dimeric Aptamers Enable the Rapid Electrochemical Detection of Wild-Type and B.1.1.7 SARS-CoV-2 in Unprocessed Saliva. *Angew. Chem., Int. Ed.* **2021**, *60* (45), 24266−24274.
(86) Sengupta, A.; Gavvala, K.; Koninti, R. K.; Hazra, P. Role of Mg2+ Ions in Flavin Recognition by RNA Aptamer. *J. Photochem. Photobiol., B* **2014**, *140*, 240−248.
(87) Rees, H. C.; Gogacz, W.; Li, N.-S.; Koirala, D.; Piccirilli, J. A. Structural Basis for Fluorescence Activation by Pepper RNA. *ACS Chem. Biol.* **2022**, *17* (7), 1866−1875.
(88) Huang, K.; Chen, X.; Li, C.; Song, Q.; Li, H.; Zhu, L.; Yang, Y.; Ren, A. Structure-Based Investigation of Fluorogenic Pepper Aptamer. *Nat. Chem. Biol.* **2021**, *17* (12), 1289−1295.
(89) Zhang, Z.; Oni, O.; Liu, J. New Insights into a Classic Aptamer: Binding Sites, Cooperativity and More Sensitive Adenosine Detection. *Nucleic Acids Res.* **2017**, *45* (13), 7593−7601.
(90) Chen, Y.-I.; Chang, Y.-J.; Liao, S.-C.; Nguyen, T. D.; Yang, J.; Kuo, Y.-A.; Hong, S.; Liu, Y.-L.; Rylander, H. G.; Santacruz, S. R.; Yankeelov, T. E.; Yeh, H.-C. Generative Adversarial Network Enables Rapid and Robust Fluorescence Lifetime Image Analysis in Live Cells. *Commun. Biol.* **2022**, *5* (1), 1−11.
(91) Qian, Y.; Cosio, D. M. O.; Piatkevich, K. D.; Aufmkolk, S.; Su, W.-C.; Celiker, O. T.; Schohl, A.; Murdock, M. H.; Aggarwal, A.; Chang, Y.-F.; Wiseman, P. W.; Ruthazer, E. S.; Boyden, E. S.; Campbell, R. E. Improved Genetically Encoded Near-Infrared Fluorescent Calcium Ion Indicators for in Vivo Imaging. *PLOS Biol.* **2020**, *18* (11), No. e3000965.
(92) Tarasov, A. I.; Griffiths, E. J.; Rutter, G. A. Regulation of ATP Production by Mitochondrial Ca2+. *Cell Calcium* **2012**, *52* (1), 28−35.
(93) Shchepina, L. A.; Pletjushkina, O. Y.; Avetisyan, A. V.; Bakeeva, L. E.; Fetisova, E. K.; Izyumov, D. S.; Saprunova, V. B.; Vyssokikh, M. Y.; Chernyak, B. V.; Skulachev, V. P. Oligomycin, Inhibitor of the F0 Part of H+-ATP-Synthase, Suppresses the TNF-Induced Apoptosis. *Oncogene* **2002**, *21* (53), 8149−8157.
(94) Symersky, J.; Osowski, D.; Walters, D. E.; Mueller, D. M. Oligomycin Frames a Common Drug-Binding Site in the ATP Synthase. *Proc. Natl. Acad. Sci. U. S. A.* **2012**, *109* (35), 13961−13965.
(95) Yetkin-Arik, B.; Vogels, I. M. C.; Nowak-Sliwinska, P.; Weiss, A.; Houtkooper, R. H.; Van Noorden, C. J. F.; Klaassen, I.; Schlingemann, R. O. The Role of Glycolysis and Mitochondrial Respiration in the Formation and Functioning of Endothelial Tip Cells during Angiogenesis. *Sci. Rep.* **2019**, *9* (1), 12608.
(96) Ren, T.-B.; Wen, S.-Y.; Wang, L.; Lu, P.; Xiong, B.; Yuan, L.; Zhang, X.-B. Engineering a Reversible Fluorescent Probe for Real-Time Live-Cell Imaging and Quantification of Mitochondrial ATP. *Anal. Chem.* **2020**, *92* (6), 4681−4688.
(97) Zhang, J.; Fei, J.; Leslie, B.; et al. Tandem Spinach Array for mRNA Imaging in Living Bacterial Cells. *Sci Rep* **2015**, *5*, 17295.
(98) Yee, T.; Furuichi, T.; Inouye, S.; Inouye, M. Multicopy Single-Stranded DNA Isolated from a Gram-Negative Bacterium, Myxococcus Xanthus. *Cell* **1984**, *38* (1), 203−209.
(99) Lim, D.; Maas, W. K. Reverse Transcriptase-Dependent Synthesis of a Covalently Linked, Branched DNA-RNA Compound in E. Coli B. *Cell* **1989**, *56* (5), 891−904.
(100) Mao, J.-R.; Shimada, M.; Inouye, S.; Inouye, M. Gene Regulation by Antisense DNA Produced in Vivo. *J. Biol. Chem.* **1995**, *270* (34), 19684−19687.
(101) Elbaz, J.; Yin, P.; Voigt, C. A. Genetic Encoding of DNA Nanostructures and Their Self-Assembly in Living Bacteria. *Nat. Commun.* **2016**, *7* (1), 11179.
(102) Chen, Y. A Novel Single-Stranded DNA Expression Vector. *Expert Opin. Biol. Ther.* **2002**, *2* (7), 735−740.
(103) Chen, Y.; McMicken, H. W. Intracellular Production of DNA Enzyme by a Novel Single-Stranded DNA Expression Vector. *Gene Ther.* **2003**, *10* (20), 1776−1780.
(104) Tan, X.-X.; Rose, K.; Margolin, W.; Chen, Y. DNA Enzyme Generated by a Novel Single-Stranded DNA Expression Vector Inhibits Expression of the Essential Bacterial Cell Division Gene ftsZ. *Biochemistry* **2004**, *43* (4), 1111−1117.
(105) Tan, X.-X.; Chen, Y. A Novel Genomic Approach Identifies Bacterial DNA-Dependent RNA Polymerase as the Target of an Antibacterial Oligodeoxynucleotide, RBL1. *Biochemistry* **2005**, *44* (17), 6708−6714.
(106) Li, J.; Wang, N.; Luo, Q.; Wan, L. The 10−23 DNA Enzyme Generated by a Novel Expression Vector Mediate Inhibition of Taco Expression in Macrophage. *Oligonucleotides* **2010**, *20* (2), 61−68.
(107) Ashton, N. W.; Bolderson, E.; Cubeddu, L.; O'Byrne, K. J.; Richard, D. J. Human Single-Stranded DNA Binding Proteins Are Essential for Maintaining Genomic Stability. *BMC Mol. Biol.* **2013**, *14* (1), 9.
(108) Wu, Y.; Lu, J.; Kang, T. Human Single-Stranded DNA Binding Proteins: Guardians of Genome Stability. *Acta Biochim. Biophys. Sin.* **2016**, *48* (7), 671−677.
(109) Karakousis, G.; Ye, N.; Li, Z.; Chiu, S. K.; Reddy, G.; Radding, C. M. The Beta Protein of Phage λ Binds Preferentially to an Intermediate in DNA Renaturation1. *J. Mol. Biol.* **1998**, *276* (4), 721−731.
(110) Muyrers, J. P. P.; Zhang, Y.; Buchholz, F.; Stewart, A. F. RecE/RecT and Redα/Redβ Initiate Double-Stranded Break Repair by Specifically Interacting with Their Respective Partners. *Genes Dev.* **2000**, *14* (15), 1971−1982.
(111) Smith, C. E.; Bell, C. E. Domain Structure of the Redβ Single-Strand Annealing Protein: The C-Terminal Domain Is Required for Fine-Tuning DNA-Binding Properties, Interaction with the Exonuclease Partner, and Recombination in Vivo. *J. Mol. Biol.* **2016**, *428* (3), 561−578.
(112) Zakharova, K.; Caldwell, B. J.; Ta, S.; Wheat, C. T.; Bell, C. E. Mutational Analysis of Redβ Single Strand Annealing Protein: Roles of the 14 Lysine Residues in DNA Binding and Recombination In Vivo. *Int. J. Mol. Sci.* **2021**, *22* (14), 7758.
(113) Zhu, Z.; Ravelet, C.; Perrier, S.; Guieu, V.; Fiore, E.; Peyrin, E. Single-Stranded DNA Binding Protein-Assisted Fluorescence Polarization Aptamer Assay for Detection of Small Molecules. *Anal. Chem.* **2012**, *84* (16), 7203−7211.
(114) Wang, Y.; Gan, N.; Zhou, Y.; Li, T.; Cao, Y.; Chen, Y. Novel Single-Stranded DNA Binding Protein-Assisted Fluorescence Aptamer Switch Based on FRET for Homogeneous Detection of Antibiotics. *Biosens. Bioelectron.* **2017**, *87*, 508−513.
(115) Xing, K.-Y.; Peng, J.; Shan, S.; Liu, D.-F.; Huang, Y.-N.; Lai, W.-H. Green Enzyme-Linked Immunosorbent Assay Based on the Single-Stranded Binding Protein-Assisted Aptamer for the Detection of Mycotoxin. *Anal. Chem.* **2020**, *92* (12), 8422−8426.
(116) Yarlagadda, V.; Medina, R.; Wright, G. D. Venturicidin A, A Membrane-Active Natural Product Inhibitor of ATP Synthase Potentiates Aminoglycoside Antibiotics. *Sci. Rep.* **2020**, *10* (1), 8134.
(117) Depaoli, M. R.; Karsten, F.; Madreiter-Sokolowski, C. T.; Klec, C.; Gottschalk, B.; Bischof, H.; Eroglu, E.; Waldeck-Weiermair, M.; Simmen, T.; Graier, W. F.; Malli, R. Real-Time Imaging of Mitochondrial ATP Dynamics Reveals the Metabolic Setting of Single Cells. *Cell Rep.* **2018**, *25* (2), 501−512 e3.

https://doi.org/10.1021/jacs.4c09855
J. Am. Chem. Soc. 2025, 147, 1529−1541